Theoretical Investigations of the Dissociation of Charged Protein Complexes in the Gas Phase

Surajith N. Wanasundara and Mark Thachuk
Department of Chemistry, University of British Columbia, Vancouver, Canada

A series of calculations, varying from simple electrostatic to more detailed semi-empirical based molecular dynamics ones, were carried out on charged gas phase ions of the cytochrome *c′* dimer. The energetics of differing charge states, charge partitionings, and charge configurations were examined in both the low and high charge regimes. As well, preliminary free energy calculations of dissociation barriers are presented. It is shown that one must always consider distributions of charge configurations, once protein relaxation effects are taken into account, and that no single configuration dominates. All these results also indicate that in the high charge limit, the dissociation of protein complex ions is governed by electrostatic repulsion from the net charges, the consequences of which are enumerated and discussed. There are two main trends deriving from this, namely that charges will move so as to approximately maintain constant surface charge density, and that the lowest barrier to dissociation is the one that produces fragment ions with equal charges. In particular, it is shown that the charge-to-mass ratio of a fragment ion is not the key physical parameter in predicting dissociation products. In fact, from the perspective of the division of total charge, many dissociation pathways reported to be "asymmetric" in the literature should be more properly labelled as "symmetric" or "near-symmetric". The Coulomb repulsion model assumes that the timescale for charge transfer is faster than that for protein structural changes, which in turn is faster than that for complex dissociation. (J Am Soc Mass Spectrom 2007, 18, 2242–2253) © 2007 American Society for Mass Spectrometry

Many experimental studies on noncovalent interactions of multimeric protein complexes have used the ESI-MS technique [1–4]. The experimental evidence indicates correlations between gas-phase and solution-phase non-covalent complexes. One challenge in using mass spectrometry for the general analysis of protein complexes is understanding the dissociation mechanism of these complexes in the gas phase. Many groups [5–19] have reported asymmetric dissociation behaviour for large multimeric proteins. A small subunit, typically a protein monomer, is ejected from the complex during dissociation, with the monomer carrying away a disproportionate amount of charge for its relative mass. Understanding the cause of this phenomenon will help to improve our understanding of the structural properties of noncovalent complexes.

It is important to investigate how these dissociations occur and the factors that influence them. Using Fourier-transform mass spectrometry (FTMS), Jurchen and Williams [6] have conducted a number of studies in order to understand the origin of these charge distributions. In these experiments, isolated charge states of cytochrome *c* dimer were dissociated by sustained off-resonance irradiation collisionally activated dissociation (SORI-CAD). According to Jurchen and Williams [6], the asymmetric charge distribution depends upon charge state, dissociation energy, and conformational flexibility. These studies showed that higher charge states lead to symmetric charge products while lower charge states lead to an asymmetric charge dissociation pathway. Further, their results with different excitation energies show that symmetric charge partitioning occurs when ions are activated using low energies while an asymmetric charge partitioning occurs at higher energies. They also observed that reducing the conformational flexibility of the proteins decreases the extent of asymmetric dissociation of the complex. Chowdhury et al. [20] pointed out that multiply charged ions are produced primarily as a result of proton attachment to the available basic sites in the protein, and that the availability of ionizable basic sites depends upon the conformation of the protein. In general, a protein in an unfolded conformation may possess more available basic sites than those in tightly folded conformations. Jurchen and Williams [6] proposed that the origin of asymmetric charge partitioning in these homodimers is the result of one of the protein monomers unfolding in the dissociation transition state.

Address reprint requests to Dr. Mark Thachuk, Department of Chemistry, University of British Columbia, 2036 Main Mall, Vancouver, BC, V6T 1Z1; Canada. E-mail: thachuk@chem.ubc.ca

© 2007 American Society for Mass Spectrometry. Published by Elsevier Inc.
1044-0305/07/$32.00
doi:10.1016/j.jasms.2007.09.022

Published online October 5, 2007
Received April 20, 2007
Revised June 21, 2007
Accepted September 17, 2007

Gas-phase collision-activated dissociation tandem mass spectrometry (CAD MS/MS) studies were carried out by Heck and co-workers for *E. coli* Glyoxalase I, human galectin, horse heart cytochrome *c*, and hen egg lysozyme [7]. They found that the charge distribution over two monomers of both Glyoxalase I and cytochrome *c* were highly asymmetric while that of both human galectin and hen egg lysozyme were a mix of symmetric and asymmetric. Smith and co-workers [10] also reported evidence for asymmetric charge distribution for streptavidin using thermally induced dissociation (TID). Smith and co-workers [10] explained their observations by giving qualitative arguments based upon the charge droplet model (CDM) proposed by Ryce and Wyman [21]. However, when Heck and co-workers [7] applied CDM to their homodimeric dissociations, it showed that equal mass fragments would obtain an equal charge. Csiszar and Thachuk [22] proposed the discretely charged ellipsoid model (DCEM) by approximating the shape of protein monomers as ellipsoids. Their results showed that charge asymmetry depends upon the relative surface area of the monomers, with charges distributing themselves to keep constant surface charge density. In other words, in the dissociation of a homodimer, if one of the monomers has more surface area than the other, DCEM would predict an asymmetric charge distribution in favour of the monomer with the higher surface area. Benesch et al. [17] have recently reported that the division of charges among the fragment ions in the dissociation of large complex ions correlates well with the relative surface areas of the products.

Klassen and coworkers [13–16] have reported a series of studies, mostly on complexes of the Shiga toxin and streptavidin complexes, in which careful thermodynamic measurements have been made employing the blackbody infrared radiative dissociation (BIRD) technique. This has been coupled with several model calculations, also based upon electrostatic calculations of charges distributed both on idealized spheres, and on protein structures. They draw conclusions that are generally consistent with previous studies, and find that their measured charge distributions can be predicted by either a simple discretely charged sphere model or by a more detailed model that includes actual protein structures incorporating monomers with varying degrees of unfolding. In other words, the charge distributions are qualitatively consistent with surface area ratios of the product ions.

To date, models of the dissociation of protein complexes have used static structures. In the current work, a series of different types of calculations are used to examine the robustness of various electrostatic models with structural changes in the protein. In other words, structural relaxations are allowed to occur, all as a function of charge state. Ultimately, the results of molecular dynamics (MD) calculations will be presented that incorporate structurally averaged effects. Molecular dynamics simulations are widely used to investigate the structure, dynamics, chemical reactivity and thermodynamics of biological molecules and their complexes in solid, liquid, and gas phases [23–25], and can provide useful information in examining the charge partitioning process.

In the first section, a bare charge model is introduced and used to seed MD simulations, whose results are discussed in the subsequent section. These calculations assert that the dynamics is strongly governed solely by the electrostatic repulsion between the charges. The discussion focuses this interpretation, bringing together those that have appeared in the literature, and produces a coherent qualitative view for the dissociation process. One consequence of this view is that by far most of the reported measurements of protein complex dissociation, especially of large ions, have followed what should be properly called a "symmetric" or "near-symmetric" fragmentation pattern. Put another way, dissociation pathways that produce fragment ions with charge to mass ratios that are asymmetric can in fact be described as symmetric if the charges on each fragment ion are the same. The present work suggests that the division of charge, not charge to mass ratio, is the more appropriate physical parameter to use when labeling a dissociation channel as symmetric or asymmetric.

Throughout this paper, the term "charge partitioning" refers to the number of charges that are assigned to each monomer in a complex ion. The term "charge configuration" refers to the particular arrangement of charges on charge sites. Thus, for a complex ion with any given total charge, several different charge partitionings are possible, and for each partitioning, many different charge configurations are possible.

Bare Charge Model

Method

The cytochrome *c′* dimer was used as the test system for the calculations. The first calculation used a simple electrostatic model in which the electrostatic repulsion between the charges in the protein are the only interactions included.

X-ray crystallographic data for the cytochrome *c′* dimer (PDB ID # bbh1) was obtained from the Protein Databank (PDB) [26]. Covey et al. [27] found that the total number of basic residues (arginine, histidine, lysine, and the N-terminus) was often similar to the maximum charge state of a protein. Smith et al. [4] also provided supporting details for this concept by compiling a list of proteins and peptides by including the maximum charge state obtained from ESI spectra and the number of basic sites. Using the same clarification, the cytochrome *c′* dimer has fifteen available basic sites on each of the two monomers. There are an enormous number of ways of distributing protons among the available basic sites for each charge state. Therefore, performing molecular dynamics simulations with all possible charge permutations is not practical.

To overcome this problem, a screening process must be

Table 1. Calculated gas phase protonation energies of the basic amino acids using the MP2/6-311+G(d,p) method

AminoAcid	Protonation Energy $\Delta E_{prot,i}$/kcal mol^{-1}
Arginine	−242.9
Histidine	−228.9
Lysine	−224.0
N-Terminus (Alanine)	−229.4

used to choose a manageable number of charge configurations. Miteva et al. [28] used a procedure based on the Metropolis algorithm for Monte Carlo sampling of charge configurations. Schnier et al. [29] developed a "pseudo-random walk" algorithm to find the lowest energy charge distributions. These studies showed that the basic sites are preferentially populated. Given that the total number of charges being considered here is always much less than the total number of basic sites, it was observed that the lowest energy distribution could always have charges located only on the basic sites.

In this study, a simple approach with bare charges was used to choose the lowest energy charge distributions. In this method, contributions from Coulomb repulsion among protonated basic sites and relative protonation energies were included in calculating relative total energies. Using the crystal structure of cytochrome c' dimer, relative total potential energies were calculated using

$$\Delta E = \sum_{i=1}^{m-1} \sum_{j=i+1}^{m} \frac{q^2}{4\pi\varepsilon_0 r_{ij}} + \sum_{i=1}^{4} n_i \Delta E_{prot,i} \quad (1)$$

in which ε_0, r_{ij}, q, and m are the permittivity of free space, distance between two charged sites, charge on the protonated sites ($q = 1$ in this study), and total number of protonated sites. The first term accounts for the Coulomb repulsion from charge-charge interactions. The protonation energy of the basic amino acids, $\Delta E_{prot,i}$, is included in order to account for the protonation energy differences between basic sites. Here, n_i is the number of residues of type i, with $i = 1, \ldots, 4$ representing arginine, histidine, lysine and the N-terminus (alanine), respectively. Protonation energies were calculated using *ab initio* methods with the Gaussian 03 program [30]. Geometry optimizations were performed with the MP2 method and the 6-311+G(d,p) basis set to obtain the total electronic energies of four protonated and non-protonated (neutral) basic amino acids in the gas phase. The electronic energy difference between the protonated and nonprotonated forms gave the protonation energies listed in Table 1. The energy ordering of calculated protonation energies is also similar to the ordering of experimentally measured affinity and basicity values [31, 32]. Note that the electrostatic calculation of eq. 1 is a crude one in that it ignores interactions between charged sites and the local protein environment. However, its use here is as a qualitative screening method only.

Results

Potential energies were first calculated by systematically constructing all possible permutations of charges among the basic sites, keeping a fixed charge partitioning between the two monomers. In other words, for the D10 charge state (with a total charge of +10 on the dimer) systems with fixed charge partitionings of M1/M9, M2/M8, M3/M7, M4/M6, and M5/M5 were formed (here Mx/My denotes x charges on one monomer and y charges on the other). For each charge partitioning, the potential energies of all possible charge locations consistent with the partitioning were evaluated using eq. 1. The potential energies were ordered from lowest to highest, and were used to identify the most favorable charge distributions for each charge partitioning. This procedure was repeated with the D18 charge state.

The lowest potential energy found for each charge partitioning from this bare charge method is plotted in Figure 1 for the D10 and D18 total charge states. In both states, relative energies increase with charge asymmetry between the two monomers. These results demonstrate that symmetric charge distributions at both charge states (D10 and D18) are energetically favoured at this level of modelling the electrostatic interactions. As well, the potential energy rises more steeply with charge asymmetry when the total charge is larger.

The total potential energy can be divided into two contributions: the intermolecular energy representing the repulsion between the two monomers, and the intramolecular energy representing the repulsion among the

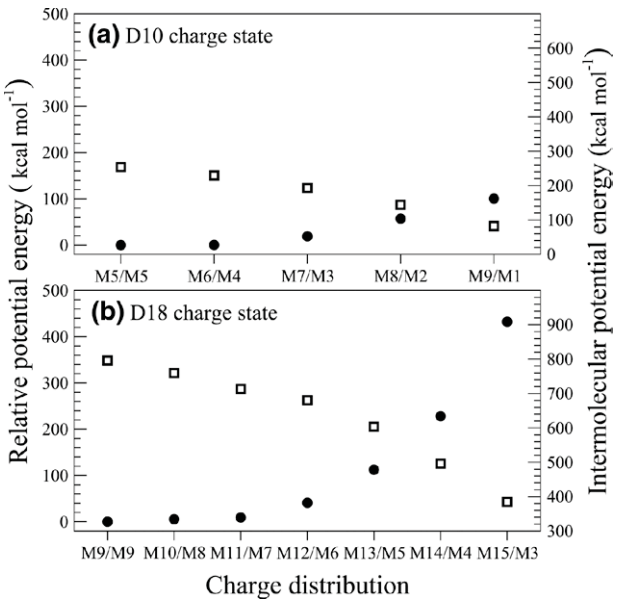

Figure 1. Relative potential energies (filled circles - read against the left vertical scale) and intermolecular potential energies (open squares - read against the right vertical scale) of the lowest energy charge configuration as a function of charge partitioning calculated using the bare charge method for the **(a)** D10 and **(b)** D18 total charge states. Here Mx/My denotes x charges on one monomer and y charges on the other.

charges within the same monomer. Intermolecular potential energies are also plotted as a function of charge partitioning for the D10 and D18 charge states in Figure 1. As the charge asymmetry grows, the intermolecular potential energy decreases while the intramolecular one increases. This of course simply reflects the fact that for asymmetric distributions, one monomer is preferentially charged, and hence incurs the greater electrostatic energy. As charge is concentrated more in a one monomer, the net repulsion between the two monomers in the dimer decreases. The key observation, which will be expanded upon below, is that the barrier for dissociation of the protein complex is governed mostly by the intermolecular potential energy.

Molecular Dynamics Simulations

Method

For each total charge state and charge partitioning, charge configurations were chosen from the bare charge calculation for further studies using MD simulations.

In this study, all MD simulations were carried out by using the Gromacs software package [33, 34]. Partial charges and force field parameters from the OPLS-AA/L force field [35] were assigned to the cytochrome *c*′ dimer. Protonated basic residual parameters are included in the published OPLS-AA/L force field but heme prosthetic group parameters are not. Therefore, in order to simulate cytochrome *c*′, we developed heme prosthetic group parameters and included them in the OPLS-AA/L force field. P_{450} heme parameters taken from the Gogonic group [36] were modified to match the heme group in cytochrome *c*′. Partial charges of the heme group and extra parameters to fit to cytochrome *c*′ were taken from heme parameters developed for the CHARMM force field by Autenrieth and co-workers [37].

To achieve the specific charge state, charges were distributed (protonated) among selected basic sites (arginine, histidine, lysine, N-terminus) with +1 net charge in each residue distributed according to the OPLS-AA/L partial charge assignment. All other amino acid residues were kept neutral. Also, the heme group and the histidine residue bonded to the heme group were not protonated. Limited memory quasi-Newton method (L-BFGS) [38] energy minimizations were carried out to remove any bad contacts between atoms before all MD simulations. All covalent bond lengths were constrained to a 0.00001 Å tolerance by the SHAKE algorithm [39]. Cutoff and periodic boundary conditions were not applied in these simulations because the system is an isolated protein dimer and no solvent is included. Initial velocities were generated according to a Maxwell-Boltzmann distribution at 300 K. The system temperature (300 K) was controlled by the Berendsen weak coupling scheme with a relaxation time constant of 0.1 ps [40].

When employing semiempirical potentials, the reference state for the zero of potential energy changes with system. Therefore, energies should be corrected according to the change in the number and location of protonated sites when different charge configurations are compared. When a neutral basic residue is protonated, the energy change should equal the protonation energy listed in Table 1. However, the OPLS-AA/L force field only partially accounts for this energy and the difference must be explicitly added. The potential energy correction term is thus

$$V_{corr} = \sum_{i=1}^{4} n_i \left(\Delta E_{prot,i} - \Delta E_{MD,i}\right) \quad (2)$$

in which $\Delta E_{MD,i}$ is the potential energy difference between the protonated and neutral amino acids after having performed L-BFGS energy minimizations of each with the OPLS-AA/L force field.

Vibrational frequencies of the bonds were not accounted for in this calculation because all bonds were kept frozen. All potential energies calculated from each MD simulation were corrected using

$$V = V_{MD} + V_{corr} \quad (3)$$

in which V_{MD} is the total MD potential energy.

Results

In order to assess the utility of the bare charge method for selecting candidate charge configurations, two particular charge states were selected, M10/M8 and M7/M3. For each of these charge states, the energies of all possible charge configurations were calculated using the bare charge method, and formed into a gaussian like distribution. From each distribution, three groups were selected: (1) the 20,000 configurations with the lowest energies (denoted "low"), (2) 6000 configurations selected from the peak of the distribution with intermediate energies (denoted "medium"), and (3) the 6000 configurations with the highest energies (denoted "high"). Short simulations (1 ps) were performed for all the configurations in each group and average potential energies were calculated over the last 0.5 ps. These potential energy values were then formed into distributions, and are plotted in Figures 2 and 3.

In the bare charge calculation, the energies of the "low," "medium," and "high" configurations are separated from each other by more than 150 kcal/mol and have a very narrow spread. The distributions in Figures 2 and 3 show mean values that still maintain the low, medium, and high energy ordering but have total widths of more than approximately 100 kcal/mol. There is substantial overlap among them, especially between the "low" and "medium" distributions. In other words, there are charge configurations that in the bare charge calculation had energies more than 100 kcal/mol above the minimum energy that relax in the short MD run to quite low energies. Stated another way, the configurations with the lowest energies in the bare charge calcu-

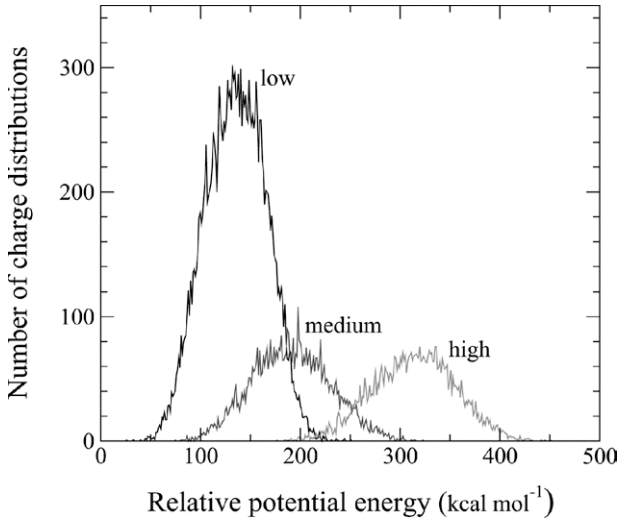

Figure 2. Distributions of relative potential energies for short run trajectories started with three groups of initial conditions, denoted "low", "medium", and "high", taken from the bare charge calculation. These results are for the M7/M3 charge partitioning of the D10 charge state.

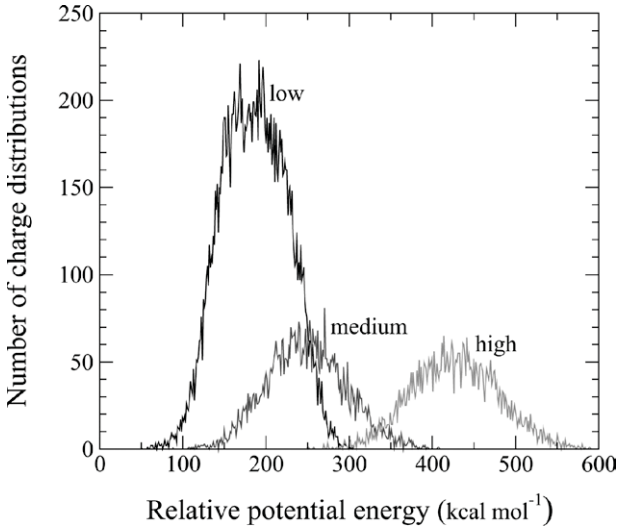

Figure 3. The same as Figure 2 except for the M10/M8 charge partitioning of the D18 charge state.

lation do not map directly to the lowest energies in the short MD calculation.

Two effects are included when moving to the short MD calculation. The first is that a better electrostatic model is used because the interactions are evaluated with the OPLS semi-empirical potential. The second is that the MD run allows small adjustments in structure to remove any interactions that are particularly repulsive (but does not allow any larger structural changes to occur). The main conclusion to be drawn from Figures 2 and 3 is that no one single charge configuration will be important but rather distributions of configurations will contribute to the behaviour of the system. The energies of these configurations are similar, and their relative ordering depends upon the particular instantaneous structure of the system. Thus, caution should be used when employing only a single structure, such as a crystal structure, to predict electrostatic energies in proteins when using an atomistic model.

For each of the D10 and D18 charge states and for each charge partitioning, the 20,000 charge configurations with the lowest energies, calculated with the bare charge method, were relaxed with short (1 ps) MD runs. From this MD set, the 50 lowest energy charge configurations were selected for longer MD runs. These simulations were conducted for up to 20 ps to better relax the system, and allow more accurate potential energy estimations to be made. Selecting only the single lowest energy charge configuration can lead to incorrect conclusions due to the limitation of sample size for short MD simulations. Fluctuations often cause the energy ordering of the configurations to change. Therefore, potential energies of the entire set of 50 charge configurations were averaged to estimate the lowest potential energy for a given charge partitioning.

The distribution of relative potential energies for different charge partitionings between two monomers in the D10 and the D18 charge states are shown in Figure 4. The energies, shown as filled squares, were calculated by averaging over time steps (energies were written every 1 fs) from 10 ps to 20 ps for each of the 50

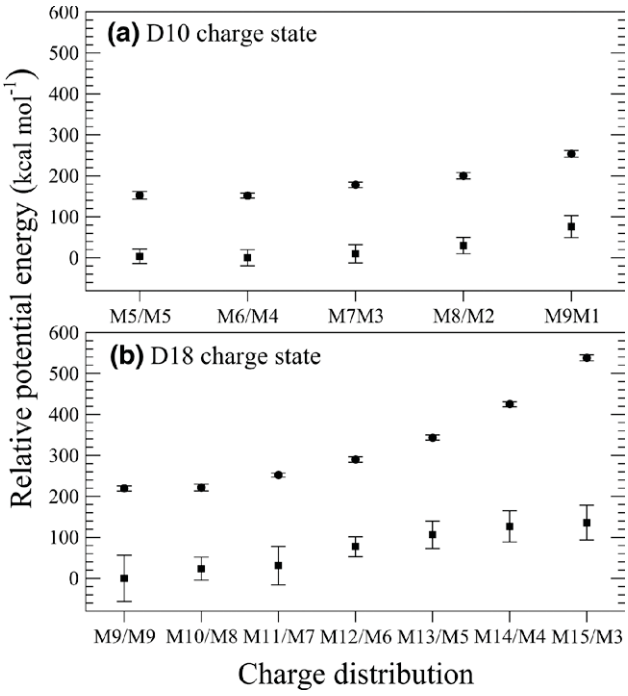

Figure 4. Averages of the relative potential energies at 1 ps (circles) and 20 ps (squares) of a MD run of an ensemble of 50 charge configurations selected with the lowest energy from the distributions in Figures 2 and 3, as a function of charge partitioning between two monomers in the **(a)** D10 and **(b)** D18 total charge states. Here Mx/My denotes x charges on one monomer and y charges on the other. The error bars indicate the widths of the distributions of the average energy of the ensemble.

charge configurations, and then averaging each of these resulting 50 energies. In addition to energy distributions from the 20 ps MD runs, the average energy distributions by averaging the same 50 configurations from 1 ps simulations are also shown as filled circles. The error bars indicate the widths of the distributions of the average energy of the ensembles of 50 trajectories. The average energies of individual trajectories are converged to statistical errors that are much less than the width of the distributions from the ensemble.

In addition to potential energy, the mean number of overcrossings [41] for the two monomers was calculated every 0.1 ps time step during the 20 ps MD run and averaged over two time intervals (0.5 to 1.0 ps and 15.0 to 20.0 ps). The change in the mean number of overcrossings is a simple geometrical descriptor to capture secondary structural changes in proteins [42]. Final values were then estimated by averaging each of 50 configurations for the two selected time intervals. Averages of the mean number of overcrossings for all charge partitionings for the D10 and D18 total charge states are listed in Table 2.

There are several observations that can be made from the data in Figure 4. First, for all cases, the potential energy is lowered by relaxations of the protein structure that can occur on the longer time scales. However, this relaxation is qualitatively different for the low (D10) and high (D18) total charge states.

For the D10 state, the energy lowering is uniform with charge partitioning so that the shape of the resulting curve is qualitatively the same both before and after relaxation. Examining the values in Table 2 shows that even after 20 ps, the average mean number of overcrossings is almost unchanged from the values at short times.

Table 2. Average mean number of overcrossings taken at 1 ps and 20 ps for MD runs of a sample of 50 charge configurations selected with the lowest energy from the distributions in Figures 2 and 3

	1 ps		20 ps	
	chain 1[a]	chain 2[a]	chain 1[a]	chain 2[a]
D10 charge state				
M5/M5	71.0 ± 0.2	70.3 ± 0.4	70.9 ± 0.5	71.2 ± 0.5
M6/M4	70.7 ± 0.5	70.8 ± 0.4	71.0 ± 0.6	71.3 ± 0.6
M7/M3	71.0 ± 0.4	70.9 ± 0.3	70.7 ± 0.6	71.5 ± 0.6
M8/M2	78.8 ± 0.2	71.1 ± 0.3	70.1 ± 0.5	71.8 ± 0.5
M9/M1	70.4 ± 0.2	71.2 ± 0.4	69.7 ± 0.5	72.0 ± 0.4
D18 charge state				
M9/M9	70.3 ± 0.3	70.5 ± 0.4	68.4 ± 1.7	69.3 ± 2.5
M10/M8	70.1 ± 0.3	70.6 ± 0.3	66.8 ± 1.7	70.5 ± 1.0
M11/M7	70.0 ± 0.3	70.8 ± 0.4	66.5 ± 2.1	70.3 ± 1.5
M12/M6	69.7 ± 0.2	70.8 ± 0.4	66.1 ± 2.0	70.7 ± 0.9
M13/M5	69.4 ± 0.3	70.7 ± 0.4	64.7 ± 1.9	70.8 ± 0.8
M14/M4	69.0 ± 0.3	70.9 ± 0.4	60.9 ± 1.9	70.9 ± 0.7
M15/M3	69.0 ± 0.2	70.9 ± 0.3	58.0 ± 2.2	70.9 ± 0.7

[a]Chains 1 and 2 denote the monomer with the higher and lower charges, respectively.

This indicates that no major structural changes have occurred. If one looks closely at the values, the values for chain 1 (the one with the higher charge) decrease slightly while those for chain 2 (the one with the lower charge) increase slightly on moving down a column for the 20 ps data. This means that the monomer with the higher charge state swells a little, and the one with the lower charge state contracts a little, as the degree of asymmetry increases.

The D18 state, on the other hand, shows qualitatively different behaviour. The lowering of the relative potential energy is higher as the asymmetric partitioning increases, as seen in Figure 4. Furthermore, the average mean number of overcrossings, seen in the 20 ps data of Table 2, decrease markedly for the monomer with the higher charge but remain constant for the monomer of lower charge. This indicates that the monomer with the higher charge state undergoes partial unfolding. This unfolding increases the monomer's surface area, and results in a lowering of the electrostatic repulsion of the charges located within it. This is the reason that the relative potential energy of the asymmetric partitioning is decreased more than that of the symmetric one by protein relaxation. The expanded monomer is not in a completely unfolded state, though. This can be seen in Figure 5 in which one trajectory from each of the ensembles was selected to give an indication of the structural changes that occur upon relaxation. The partial unfolding of the monomer with the greater charge in the D18 state is evident. Again, it must be emphasized that these structures are not unique, and that different trajectories in the ensemble relax to differing structures. Finally, it should also be noted that on the timescale of these calculations, many of the symmetric charge state species promptly dissociated (with little unfolding occurring during the dissociation event) while the asymmetric ones remained bound.

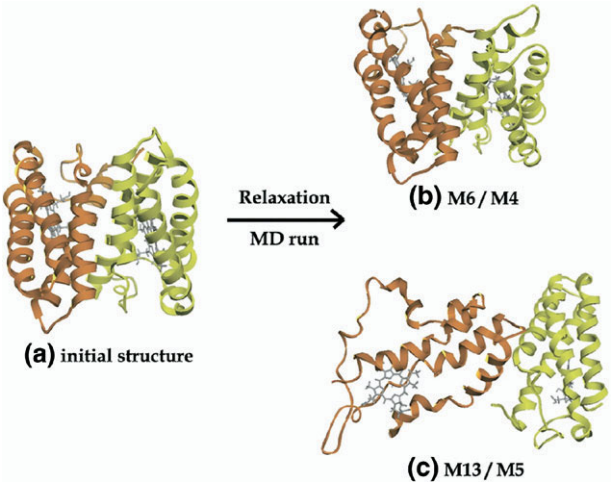

Figure 5. Snapshots of cytochrome *c*′ structures initially **(a)** and after a 20 ps MD simulation with the (**b**) M6/M4, and (**c**) M13/M5 charge partitioning. In each complex, the higher and lower charged monomers are drawn to the left and right, respectively.

The second observation concerns the widths of the distributions of relative energies, indicated by the bars on the data points in Figure 4. Each individual trajectory has a well-converged average energy. The ensemble of 50 trajectories though has a distribution of energies, whose mean is plotted as filled circles, and whose widths are represented by the bars. Again, the energy ordering of the states changes upon protein relaxation. However, for the lower charge state, the band of energies for M5/M5, M6/M4, and M7/M3 overlap almost completely. This implies that there are manifolds of different charge partitioning and configurations that, upon protein relaxation, have similar energies. In other words, for low charge states, the monomers act as sponges, able to absorb a certain number of charges without any noticeable change in structure or energy. This implies that there is no single charge partitioning or configuration that dominates the behavior of the system, and one should not extrapolate results from any single structure (such as a crystal structure). Also, at low charge states, a fair degree of asymmetry can be energetically stabilized, even in the absence of any significant change in the structure of the complex.

For the higher charge state though, this breaks down due both to the extra Coulomb repulsion present in the system, and to the decreased flexibility in the choice of sites to locate charges, so that even after accounting for the widths of the distributions, the symmetric distribution is still energetically favored.

Discussion

Coulomb Repulsion Model

The MD results presented here use more realistic electrostatic models than had been used in our previous study of ellipsoids [22] but point to essentially the same conclusions, namely that the system is governed predominantly by electrostatic repulsions between the net charges. This, of course, is not a novel statement and has been made by several researchers examining this phenomena. For example, Kaltashov and Mohimen [43] demonstrated a correlation between the total charge and the solvent accessible surface area of proteins in the ESI-MS process. However, it is worth enumerating the consequences of this model because the full extent of it has not been employed.

The Coulomb repulsion model predicts two general trends.

A. Charges that are free to move adopt the lowest energy when uniformly spread over the surface of an object, with a slight concentration among the points that are furthest apart if polarization effects are accounted for. To remain at lowest energy, the surface charge density should be kept constant.
B. For an object, such as a protein complex ion that is a collection of like objects bound together, all other interactions being equal, to the extent that Coulomb intermolecular repulsion dominates, the lowest energy barrier for dissociation occurs when all fragment ions have the same charge, that is the total charge is divided symmetrically among the fragment ions.

The second trend follows simply from the fact that the long-range repulsion among charges is greatest for the symmetric case. For example, for a complex that dissociates into two fragments with charges q_1 and q_2, the long-range repulsion, $q_1q_2 / 4\pi\epsilon_0 r$, is a maximum when $q_1 = q_2 = n/2$ (if $q_1 + q_2 = n$), and progressively decreases as the difference between q_1 and q_2 increases. This can be seen in Figure 6 in which preliminary free energy curves calculated with molecular dynamics methods are shown as a function of the distance between the centers of mass of the two monomers for the D10 state with a number of different charge partitionings. As the charge asymmetry increases, so does the barrier to dissociation. This is also consistent with the experimental results of Sinelnikov et al. [15] who assert that the long-range repulsion between charged groups dominate the dissociation of a number of protein complexes, and who sought to understand the relationship between measured activation energies and some calculated values of this repulsion.

It should also be noted that this long-range repulsion is generally the same regardless of how the charges q_1 and q_2 are distributed, since the repulsion between two uniformly charged spheres with charges q_1 and q_2 is the same as that between two point charges. In other words, the barrier to dissociation is determined by the absolute total charge, not on the surface charge density.

When considering protein complexes, it is important

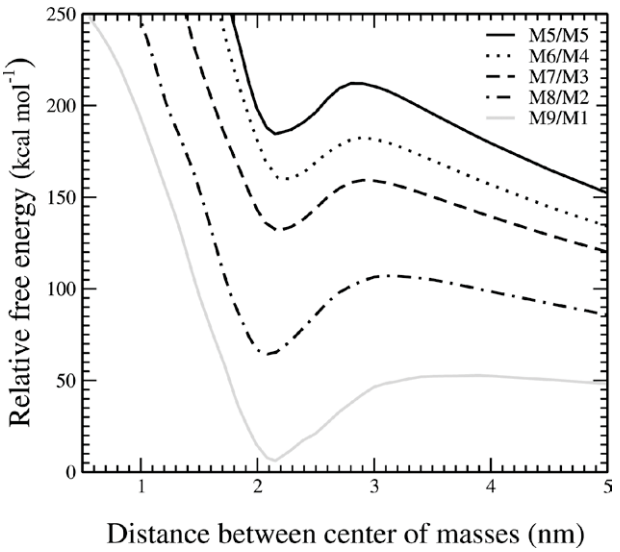

Figure 6. Free energies as a function of the distance between the centers of mass of the two monomers in the cytochrome *c*′ dimer with a total charge of +10 for differing charge partitioning. The curves have arbitrarily had their asymptotic values all set to the same zero. As the charge partitioning becomes more symmetric, the free energy barrier to dissociation decreases.

to stress that the minimum electrostatic state in Trend A is never reached in practice because the charges in proteins are mostly localized at particular sites, so are unable to spread into a layer of uniform charge density. Thus, all charge configurations in protein complexes have energies higher than this global minimum, so in principle can have their energies changed relative to one another by relaxation processes. In other words, a charge distribution that is slightly nonuniform might be relaxed enough by protein structural changes to have the same energy as one that is more uniform. This is the reason that states of differing charge configuration and partitioning, as seen in Figure 4, can exist at approximately the same energy. Thus, in protein complexes there will always be fluctuations around the constant charge density limit of Trend A. This result is consistent with the calculations using charged ellipsoids [22], in which case fluctuations of 10% to 15% were observed from the constant surface charge density state.

Finally, Trend A depends upon the mutual repulsion of charges within a complex, which in turn depends upon the surface charge density. The greater the surface charge density, the greater will be this Coulomb energy relative to other interactions in the complex, and the more Trend A should dominate. On the other hand, Trend B should dominate as the total charge on the complex increases. In typical protein complexes, the binding energy holding a given monomer in a complex does not scale with the size of the complex but rather depends only upon a constant number of binding interactions. However, the charge that can be imparted to such a complex grows with its size. Thus, the repulsion between the charges can quickly dominate as a complex grows larger. Note that this is different from the underlying principles involved with charged droplet or fission models. In those cases, Coulomb repulsion is balanced by surface tension, and the latter does scale with surface area. The balance between these two forces then determines the behavior of the system. Finally, in principle, the surface charge density and total charge can be varied independently.

Application of the Coulomb Repulsion Model

Consider for a moment the application of the Coulomb repulsion model to large, multimeric complexes. In many cases, large multimeric complexes are produced with high charges but small charge per monomer ratios, that is, small surface charge densities. In this case, one expects Trend B to dominate while there may be fluctuations around the limit suggested by Trend A. In the equilibrium state, a complex composed of the same monomers with a total of n charges should exist in a state in which the charges are generally evenly distributed among the complex, as suggested by Trend A. However, as seen in Figure 4, because the surface charge density is typically low, it is expected that a range of charge partitionings will be present, with some monomers in the complex, at any given time, having a slight concentration of charge but undergoing small relaxations to stabilize them. That is, the complex ions should be composed of a range of charge configurations and partitionings close to evenly-distributed but also with some asymmetry.

When energy is imparted to such a complex, through SORI-CAD, BIRD, or other gentle heating techniques, the internal energy slowly increases. Those complexes that in the equilibrium state have one monomer with a slight charging are expected to be affected first since the greater intramolecular repulsion present in these monomers will make them more susceptible to conformational changes. These conformational changes can eventually cause these monomers to be ejected from the complex, much like the strength of a chain is determined by its weakest link. This, we postulate, is the main reason experimental studies show that multimeric complexes tend to dissociate almost exclusively by losing only a single monomer at a time.

As the internal energy increases, a complex has many dissociation channels available for different charge partitionings and configurations. If the energy increase is slow relative to the timescales of protein structural changes, the lowest energy barrier will be, according to Trend B, the one that divides the charge evenly. However, in order for this dissociation pathway to be accessible, in accordance with Trend A, the surface areas of the two dividing fragments must be approximately the same. If a monomer divides from a multimeric complex, it must partially or completely unfold up to the point where its surface area equals that of the other fragment ion in the dissociation channel. The proposal that monomer unfolding is inherent in the dissociative pathway has been put forth by several research groups [10, 14] and examined in particular detail by Jurchen and Williams [6]. We employ this idea as a means of explaining how surface charge density can be kept constant during the dissociation process. If, either due to structural constraints within the monomer that limit unfolding, or due to a size disparity between the remaining fragment ion and the fully unfolded monomer, the surface areas of the monomer and remaining fragment ion cannot be made the same, then the symmetric charge dissociation pathway will be inaccessible.

In this case, the system tries to get as close to the symmetric limit as possible by putting as much charge on the departing monomer as allowed by its surface area, according to Trend A. Thus, the ratio of the surface area of the unfolded ejected monomer to that of the remaining complex should give a reasonably good approximation of the charge ratio between the two.

These scenarios have been observed experimentally. For example, tetrameric complexes of protonated streptavidin ions are found to fragment in a symmetric fashion, [10, 15] with S_4^{+n} ions producing predominantly $S_3^{+n/2}$ and $S^{+n/2}$ fragments, with n varying between 14 and 18. Fluctuations around these limits of one unit of charge are also observed. This indicates that one streptavidin monomer is sufficiently flexible so as to unfold to produce a surface area commensurate with

the remaining trimer fragment ion. This interpretation is consistent with the electrostatic model calculations of Sinelnikov et al. [15], who showed that a partially unfolded monomer subunit could account for the observed charge ratios. Interpreted in another way, the monomer need unfold only to the extent of making its surface area commensurate with the remaining trimer fragment ion.

Similar results have been measured for the dissociation of the tetrameric complex transt-hyretin (TTR) by Sobott et al. [18]. They dissociate complex ions with +15 charge and observe that the dominant dissociation pathway produces monomer ions of charge +8 and trimer ions of charge +7. In addition, monomer ions of charge +9 and +7 are also observed. Thus, in this case symmetric charge dissociation is observed, consistent with predictions of the Coulomb repulsion model.

For pentameric complexes of the Shiga toxins, the results of Klassen and coworkers [13–15] are slightly different. The +14 charge state complex divides into a monomer and tetramer with a broad range of partitionings around a dominant channel which has a monomer being ejected with charge +6. The symmetric channel has very low population. In this case, the Coulomb repulsion model would rationalize that the complex has not been able to reach the symmetric limit because the monomer has not been able to unfold to a state with surface area large enough to match the tetrameric fragment. The dissociation is "near symmetric" though, in that the division of charge is close to the symmetric limit. The electrostatic calculations of Sinelnikov et al. [15] support this interpretation. In that work, a partially unfolded structure is found to reproduce the experimental charge partitioning, and this is physically attributed to a disulfide bond in the monomers which prevent complete unfolding. However, in addition, they estimated the charge partitioning in the limit of complete unfolding by breaking this bond, in their fully unfolded protein structure model (FU-PSM). The reported values, shown in the last column of Table 2 in reference 15, are almost precisely half the total charge state of the original Shiga toxin complexes. In other words, if the monomer were able to completely unfold, the symmetric dissociation channel would be the dominant one.

The measurements of Sinelnikov et al. [15] are particularly interesting because they examine both positive and negative total charge states of the Shiga toxin complexes. Generally, they find that the charge fragmentation channels are the same, regardless of the sign of the charge on the complex. Again, this is consistent with the Coulomb repulsion model, since the long-range dissociation repulsion depends only upon the product of the charges on the fragment ions, and not on their absolute signs. Trend B would predict the same dissociation barrier for complexes with the same total charge but differing signs.

Larger multimeric complexes behave in a similar way. Robinson and coworkers [17, 19] have studied 12-mers of *Ta*HSP16.9 and 24-mers of *Mj*HSP16.5 at high charge states (approximately +2 charges per monomer). Again, because the surface charge density is low, it is expected that fluctuations around uniform charge partitioning will be present in the unperturbed ions, and that some complexes will contain monomers that are charged higher than the average. These are the ones that are expected to be most susceptible to dissociation when energy is added to the system.

The large charges on these complexes should make Trend B dominate. Thus, the complexes should try to dissociate into fragments of equal charge and surface area. However, because the complexes are so large, even completely unfolded monomers will not have surface areas equal to the remaining complex fragment ions. In this situation, the model predicts the charge partitioning between monomer and complex fragment ions to equal the ratio of surface areas of the two. This prediction is consistent with reported surface area ratio calculations [17]. In fact, it was observed experimentally that an n-mer complex ion can lose a single monomer ion, with the resulting $(n - 1)$-mer fragment ion again dissociating by losing a single monomer ion to produce a lower charged $(n - 2)$-mer complex ion. In each case, the ratio of surface areas of the complex ion and unfolded ejected monomer ion approximated the charge partitioning among the fragments. This behavior is also consistent with the Coulomb repulsion model. After ejecting a single monomer, a complex ion may still have a substantial charge, and thus still be dominated by electrostatic interactions. One then expects precisely the same behavior as with the original complex, namely additional loss of a monomer with the system attempting to attain as close to symmetric charge distribution as possible. This process is expected to repeat itself until the total charge of the remaining fragment complex ion is low enough that other interactions begin to compete with Coulomb repulsion.

Heck and coworkers [44] reported interesting dissociation behaviour for the dissociation of tetrameric complexes of 2-keto-3-deoxyarabinonate dehydratase. These complexes dissociate almost exclusively into two dimeric fragment ions rather than the usual loss of a single monomer. The complexes are composed of dimers that have more binding interactions internally than between them, making them more prone to dissociate into dimeric fragments. They found in fact that the complexes are quite susceptible to dissociation. The key observation though is that the dimers are produced with near symmetric charges. This is completely consistent with Trend B which predicts that symmetric charge partitioning should dominate regardless of how a complex breaks into fragments.

It should be emphasized that charge-to-mass ratio is not a relevant parameter in determining the charge partitioning of multimeric ions. The relevant parameters are total charge on the ion, and surface charge density. So, for example, the dissociation of the tetrameric streptavidin ion into monomer and trimer ions

of equal charge has been classified as an asymmetric dissociation because the charge to mass ratios of the resulting fragments are very different. However, within the Coulomb repulsion model, this dissociation would in fact be classified as symmetric, because the charge division is equal.

All the arguments above hinge upon two important assumptions: (1) that charge transfer is labile (and that sufficient charge sites are available), and (2) that monomer conformational changes occur on a timescale that is faster than the dissociation timescale. A number of experimental measurements [14, 15, 45–48] indicate that indeed charge transfer in proteins is labile. Some theoretical calculations [49–51] also indicate that proton migration along the backbone may be a likely mechanism for charge transfer. However, changing experimental conditions in such a way as to weaken these two assumptions will also weaken the general predictions of the Coulomb repulsion model.

For example, Felitsyn et al. [16] have reported measurements of the dissociation of ecotin dimer ions with high charges (+14 to +17). One would expect the Coulomb repulsion model to be applicable, and that symmetric dissociation is expected. However, while the symmetric dissociation channel was indeed observed, there was also significant population in channels that deviated from symmetry by one and two units of charge. The time dependence of the fragment distributions indicated that evidence for charge transfer was not strong. It was concluded that the different dissociation channels reflected the distribution of charge partitioning among the monomers in the original complex ions. This is completely consistent with the phenomena shown in Figure 4 in which fluctuations about the symmetric distribution are expected simply due to local relaxation effects. If these dimers dissociate without charge transfer occurring, then one would expect to reveal the distribution of charge partitioning present in the equilibrium state which is distributed about the symmetric one. Note that during the ESI process, charges are expected to be mobile before the naked ion is produced. Thus, the equilibrium state is expected to be established in the complex, even if charge transfer is inhibited afterwards.

This is also seen in the surface-induced dissociation (SID) experiments of Wysocki and coworkers [8] in which ions are dissociated into fragments on a picosecond timescale by colliding them with a surface. This causes fragmentation to occur on a timescale that is faster than that for conformational changes in the monomers. For SID of cytochrome *c* dimers of charge +11, monomer fragments with charges +5 and +6 dominate. That is, a symmetric charge distribution is observed. In general, if experimental conditions are used that dissociate ions quickly compared with the timescale for monomer conformational changes, the Coulomb repulsion model predicts that each monomer in a complex should have approximately the same charge. Thus, monomers ejected from an *n*-mer would be expected to carry a charge of approximately $1/n$ of the total charge on the complex. In such a cases for $n \neq 2$, the dissociation channel would be labelled as "asymmetric" within the Coulomb repulsion model because the fragment ions have differing charges, even though the charge to mass ratios of the fragment ions would be the same.

The Coulomb repulsion model is also consistent with the detailed experiments performed by Jurchen and Williams [6] that showed, among other things, the relationship between monomer flexibility and the degree of asymmetry in fragment ions. In particular, monomers with greater rigidity led preferentially to symmetrically charged dissociation products. Considering Trends A and B, rigid monomers are not able to change their surface areas much, due to conformational constraints.

Note that in all cases, one would never expect to see a multimeric complex ion dissociate by ejecting a monomer with greater than half the total charge on the complex (apart from small fluctuations).

Deviations from symmetric charge dissociation can be expected for ions with lower charge states because other interactions compete with the Coulomb repulsion among the net charges. In this case, a more complicated dissociation mechanism is at work. It may happen that even the symmetric distribution of charge produces a barrier that is high relative to the internal energy, and the system needs to find another pathway for dissociation.

Asymmetric charge distributions lower the intermolecular repulsion but increase the intramolecular repulsion. In order for dissociation to occur, typically hydrogen bond interactions in the protein complex must be broken. Greater intramolecular repulsion can promote conformation changes in a monomer that increase its size, and thereby may weaken hydrogen bonds that bind the complex. In this way, the lowest energy path for dissociation can be through unfolding-like transition states encouraged by asymmetric charge distributions, as has been postulated by several groups [7, 10, 14, 15]. Currently, we are performing detailed calculations of potentials of mean force to investigate such mechanisms in some detail.

Conclusion

Simplified charge calculations, as well as finer, atomistic level semi-empirical calculations using molecular dynamics were performed for the cytochrome *c*′ dimer in the gas phase. These calculations showed that overall, the behavior could be explained by an electrostatic model based upon the repulsion between the net charges on the protein. This model, when extended to protein complexes, predicts that charges should seek to arrange themselves so as to maintain approximately a uniform surface charge density, and that the smallest barrier to dissociation should occur when a complex dissociates into fragments, each carrying the same charge. These predictions rely upon the assumption that charge transfer is labile and that the timescale for

dissociation is slower than that for conformational changes. Several groups have used similar electrostatic arguments to model experimental results [15, 17], and this model is consistent with many of these arguments. However, to date the full ramifications of this model have not been recognized, such as that a symmetric distribution of charge is predicted, regardless of the charge-to-mass ratio of a fragment ion. From this perspective, many dissociation pathways that have been labeled "asymmetric" in the literature would actually be "symmetric" ones within the Coulomb repulsion model.

In practice, the Coulomb repulsion model will be poorer for complexes with low charges. In this case, the interactions within a complex compete with the repulsion between its charges. We are currently performing free energy calculations to study the dissociation mechanism for this case in more detail.

Acknowledgments

The authors gratefully acknowledge support for this work by a grant from the National Sciences and Engineering Research Council (NSERC) of Canada. All computations were performed by using WestGrid computing resources, which are funded in part by the Canada Foundation for Innovation, Alberta Innovation and Science, BC Advanced Education, and the participating research institutions http://www.westgrid.ca.

References

1. Veenstra, T. D. Electrospray Ionization Mass Spectrometry in the Study of Biomolecular Noncovalent Interactions. *Biophys. Chem*. **1999,** *79,* 63–75.
2. Kebarle, P. A. Brief Overview of the Present Status of the Mechanisms involved in Electrospray Mass Spectrometry. *J. Mass Spectrom*. **2000,** *35,* 804–817.
3. Cole R. B. Electrospray Ionization Mass Spectrometry. Wiley: New York, 1997.
4. Smith, R. D.; Loo, J. A.; Loo, R. R. O.; Busman, M.; Udseth, H. R. Principles and Practice of Electrosparay Ionization-Mass Spectrometry for Large Polypeptides and Proteins. *Mass Spectrom. Rev*. **1991,** *10,* 359–452.
5. Jurchen, J. C.; Garcia, D. E.; Williams, E. R. Gas-Phase Dissociation Pathways of Multiply Charged Peptide Clusters. *J. Am. Soc. Mass Spectrom*. **2003,** *14,* 1373–1386.
6. Jurchen, J. C.; Williams, E. R. Origin of Asymmetric Charge partitioning in the Dissociation of Gas-Phase Protein Homodimers. *J. Am. Chem. Soc.* **2003,** *125,* 2817–2826.
7. Versluis, C.; van der Staaij, A.; Stokvis, E.; Heck, A. J. R.; Craene, B. Metastable Ion Formation and Disparate Charge Separation in the Gas-Phase Dissection of Protein Assemblies Studied by Orthogonal Time-of-Flight Mass Spectrometry. *J. Am. Soc. Mass Spectrom*. **2001,** *12,* 329–336.
8. Jones, C. M.; Beardsley, R. L.; Galhena, A. S.; Dagan, S.; Cheng, G.; Wysocki, V. H. Symmetrical Gas-Phase Dissociation of Noncovalent Protein Complexes via Surface Collisions. *J. Am. Chem. Soc*. **2006,** *128,* 15044–15045.
9. Versluis, C.; Heck, A. J. R. Gas-Phase Dissociation of Hemoglobin. *Int. J. Mass Spectrom.* **2001**, *210/211*, 637–649.
10. Schwartz, B. L.; Bruce, J. E.; Anderson, G. A.; Hofstadler, S. A.; Rockwood, A. L.; Smith, R. D.; Chilkoti, A.; Stayton, P. S. Dissociation of Tetrameric Ions of Noncovalent Streptavidin Complexes Formed by Electrospray Ionization. *J. Am. Soc. Mass Spectrom*. **1995,** *6,* 459–465.
11. Iavarone, A. T.; Williams, E. R. Collisionally Activated Dissociation of Supercharged Proteins Formed by Electrospray Ionization. *Anal. Chem.* **2003,** *75,* 4525–4533.
12. Jurchen, J. C.; Garcia, D. E.; Williams, E. R. Further Studies on the Origins of Asymmetric Charge Partitioning in Protein Homodimers. *J. Am. Soc. Mass Spectrom*. **2004,** *15,* 1408–1415.
13. Sinelnikov, I.; Kitova, E. N.; Klassen, J. S.; Armstrong, G. D. Effects of Single Amino Acid Substitution on the Dissociation of Multiply Charged Multiprotein Complexes in the Gas Phase. *J. Am. Soc. Mass Spectrom*. **2007,** *18,* 688–692.
14. Felitsyn, N.; Kitova, E. N.; Klassen, J. S. Thermal Decomposition of a Gaseous Multiprotein Complex Studied by Blackbody Infrared Radiative Dissociation. Investigating the Origin of the Asymmetric Dissociation Behavior. *Anal. Chem.* **2001,** *73,* 4647–4661.
15. Sinelnikov, I.; Kitova, E. N.; Klassen, J. S. Influence of Coulombic Repulsion on the Dissociation Pathways and Energetics of Multiprotein Complexes in the Gas Phase. *J. Am. Soc. Mass Spectrom.* **2007,** *18,* 617–631.
16. Felitsyn, N.; Kitova, E. N.; Klassen, J. S. Thermal Dissociation of the Protein Homodimer Ecotin in the Gas Phase. *J. Am. Soc. Mass Spectrom.* **2002,** *13,* 1432–1442.
17. Benesch, J. L. P.; Aquilina, J. A.; Ruotolo, B. T.; Sobott, F.; Robinson, C. V. Tandem Mass Spectrometry Reveals the Quaternary Organization of Macromolecular Assemblies. *Chem. Biol*. **2006,** *13,* 597–605.
18. Sobott, F.; McCammon, M. G.; Robinson, C. V. Gas-Phase Dissociation Pathways of a Tetrameric Protein Complex. *Int. J. Mass Spectrom*. **2003,** *230,* 193–200.
19. Benesch, J. L. P.; Sobott, F.; Robinson, C. V. Thermal Dissociation of Multimeric Protein Complexes by Using Nanoelectrospray Mass Spectrometry, *Anal. Chem*. **2003,** *75,* 2208–2214.
20. Chowdhury, S. K.; Katta, V.; Chait, B. T. Probing Conformational Changes in Proteins by Mass Spectrometry. *J. Am. Chem. Soc*. **1990,** *112,* 9012–9013.
21. Ryce, S. A.; Wyman, R. R. Two Sphere for the Asymmetric Division of Electrically Charged Liquid Drops. *Can. J. Phys.* **1970,** *112,* 2571–2576.
22. Csiszar, S.; Thachuk, M. Using Ellipsoids to Model Charge Distributions in Gas Phase Protein Complex Ion Dissociation. *Can. J. Chem*. **2004,** *82,* 1736–1744.
23. Allen, M. P., Tildesley, D. J. Computer Simulation of Liquids. Clarendon Press: New York, NY, 1989.
24. Haile J. M. Molecular Dynamics Simulation: Elementary Methods. John Wiley and Sons Inc.: New York, 1992.
25. Wan, W.; Donini, O.; Reyes, C. M.; Kollman, P. A. Biomolecular Simulations: Recent Developments in Force Fields, Simulations of Enzyme Catalysis, Protein-Ligand, Protein-Protein, and Protein-Nucleic Acid Noncovalent Interactions. *Annu. Rev. Biophys. Biomol. Struct.* **2001,** *30,* 211–243.
26. Ren, Z.; Meyer, T.; McRee, D. E. PDB ID:1bbh. Atomic Structure of a Cytochrome *c*′ with an Unusual Ligand-Controlled Dimer Dissociation at 1.8 A Resolution. *J. Mol. Biol.* **1993,** *234,* 433–445.
27. Covey, T. R.; Bonner, R. F.; Shushan, B. I.; Henion, J.; Boyd, R. K. The Determination of Protein, Oligonucleotide and Peptide Molecular Weights by Ion-Spray Mass Spectrometry. *Rapid Commun. Mass Spectrom.* **1988,** *2,* 249–256.
28. Miteva, M.; Demirev, P. A.; Karshikoff, A. D. Multiply-Protonated Protein Ions in the Gas Phase: Calculation of the Electrostatic Interactions between Charge Sites. *J. Phys. Chem. B.* **1997,** *101,* 9645–9650.
29. Schnier, P. D.; Gross, D. S.; Williams, E. R. On the Maximum Charge State and Proton Transfer Reactivity of Peptide and Protein Ions Formed By Electrospray Ionization. *J. Am. Soc. Mass Spectrom.* **1995,** *6,* 1086–1097.
30. Frisch, M. J.; Trucks, G. W.; Schlegel, H. B.; Scuseria, G. E.; Robb, M. A.; Cheeseman, J. R.; Montgomery, J. A. Jr.; Vreven, T.; Kudin, K. N.; Burant, J. C.; Millam, J. M.; Iyengar, S. S.; Tomasi, J.; Barone, V.; Mennucci, B.; Cossi, M.; Scalmani, G.; Rega, N.; Petersson, G. A.; Nakatsuji, H.; Hada, M.; Ehara, M.; Toyota, K.; Fukuda, R.; Hasegawa, J.; Ishida, M.; Nakajima, T.; Honda, Y.; Kitao, O.; Nakai, H.; Klene, M.; Li, X.; Knox, J. E.; Hratchian, H. P.; Cross, J. B.; Bakken, V.; Adamo, C.; Jaramillo, J.; Gomperts, R.; Stratmann, R. E.; Yazyev, O.; Austin, A. J.; Cammi, R.; Pomelli, C.; Ochterski, J. W.; Ayala, P. Y.; Morokuma, K.; Voth, G. A.; Salvador, P.; Dannenberg, J. J.; Zakrzewski, V. G.; Dapprich, S.; Daniels, A. D.; Strain, M. C.; Farkas, O.; Malick, D. K.; Rabuck, A. D.; Raghavachari, K.; Foresman, J. B.; Ortiz, J. V.; Cui, Q.; Baboul, A. G.; Clifford, S.; Cioslowski, J.; Stefanov, B. B.; Liu, G.; Liashenko, A.; Piskorz, P.; Komaromi, I.; Martin, R. L.; Fox, D. J.; Keith, T.; Al-Laham, M. A.; Peng, C. Y.; Nanayakkara, A.; Challacombe, M.; Gill, P. M. W.; Johnson, B.; Chen, W.; Wong, M. W.; Gonzalez, C.; and Pople, J. A. *Gaussian 03, Revision* B.05; Gaussian, Inc.: Wallingford CT, 2004.
31. Harrison, A. G. The Gas-Phase Basicities and Proton Affinities of Amino Acids and Peptides. *Mass Spectrom. Rev.* **1997,** *16,* 201–217.
32. Wu, Z.; Fenselau, C. Proton Affinity of Arginine Measured by the Kinetic Approach. *Rapid Commun. Mass Spectrom.* **1992,** *6,* 403–405.
33. Berendsen, H. J. C.; van der Spoel, D.; van Drunen, R. GROMACS: A Message-Passing Parallel Molecular Dynamics Implementation. *Comp. Phys. Commun.* **1995,** *91,* 43–56.
34. Lindahl, E.; Hess, B.; van der Spoel, D. GROMACS 3.0: A Package for Molecular Simulation and Trajectory Analysis *J. Mol. Mod.*. **2001,** *7,* 306–317.
35. Kaminski, G. A.; Friesner, R. A.; Tirado-Rivers, J.; Jorgensen, W. L. Evaluation and Reparametrization of the OPLS-AA Force Field for Proteins via Comparison with Accurate Quantum Chemical Calculations on Peptides. *J. Phys. Chem. B.* **2001,** *105,* 6474–6487.
36. Gogonea, V.; Shy, J. M. II.; Biswas, P. K. Electronic Structure, Ionization Potential, and Electron Affinity of the Enzyme Cofactor (6R)-5,6,7,8-Tetrahydrobiopterin in the Gas Phase, Solution, and Protein Environments. *J. Phys. Chem. B*. **2006,** *110,* 22861–22871.

37. Autenrieth, F.; Tajkhorshid, E.; Baudry, J.; Luthey-Schulten, Z. Classical Force Field Parameters for the Heme Prosthetic Group of Cytochrome *c*. *J. Comput. Chem*. **2004,** *25,* 1613–1622.
38. Liu, D. C.; Nocedal, J. On the Limited Memory BFGS Method for Large Scale Optimization. *Math. Prog*. **1989,** *48,* 503–528.
39. Kräutler, V.; Van Gunsteren, W. F.; Hünenberger, P. H. A Fast SHAKE Algorithm to Solve Distance Constraint Equations for Small Molecules in Molecular Dynamics Simulations. *J. Comput. Chem. 22,* **2001,** 501–508.
40. Berendsen, H. J. C.; Postma, J. P. M.; Van Gunsteren, W. F.; DiNola, A.; Haak, J. R. Molecular Dynamics with Coupling to an External Bath. *J. Chem. Phys.* **1984,** *81,* 3684–3690.
41. Arteca, G. A. Path-Integral Calculation of the Mean Number of Overcrossings in an Entangled Polymer Network. *J. Chem. Inf. Comput. Sci*. **1999,** *39,* 550–557.
42. Arteca, G. A.; Tapia, O. Structural Transitions in Neutral and Charged Protein in vacuo. *J. Mol. Graphics Model*. **2001,** *19,* 102–118.
43. Kaltashov, I. A.; Mohimen A. Estimates of Protein Surface Areas in Solution by Electrspray Ionization Mass Spectrometry. *Anal. Chem*. **2005,** *77,* 5370–5379.
44. Van den Heuvel, R. H. H.; Van Duijn, E.; Mazon, H.; Synowsky, S. A.; Lorenzen, K.; Versluis, C.; Brouns, S. J. J.; Langridge, D.; Van der Oost, J.; Hoyes, J.; Heck, A. J. R. Improving the Performance of a Quadrupole Time-of-Flight Instrument for Macromolecular Mass Spectrometry. *Anal. Chem.* **2006**, 78, 7473–7483.
45. Kohtani, M.; Jones, T. C.; Sudha, R.; Jarrold, M. F. Proton Transfer-Induced Conformational Changes and Melting in Designed Peptides in the Gas Phase. *J. Am. Chem. Soc*. **2006,** *128,* 7193–7197.
46. Dongré, A. R.; Jones, J. L.; Somogyi, A.; Wysocki, V. H. Influence of Peptide Composition, Gas-Phase Basicity, and Chemical Modification on Fragmentation Efficiency: Evidence for the Mobile Proton Model. *J. Am. Chem. Soc*. **1996,** *118,* 8365–8374.
47. Wysocki, V. H.; Tsaprailis, G.; Smith, L. L.; Breci, L. A. Mobile and Localized Protons: A Framework for Understanding Peptide Dissociation *J. Mass Spectrom*. **2000,** *35,* 1399–1399.
48. Vaisar, T.; Urban, J. Gas-phase Fragmentation of Protonated Mono-N-Methylated Peptides. Analogy with Solution-Phase Acid-Catalyzed Hydrolysis. *J. Mass Spectrom.* **1998,** *33,* 505–524.
49. Marinica, D. C.; Grégoire, G.; Desfrançois, C.; Schermann, J. P.; Borgis, D.; Gaigeot, M. P. Ab Initio Molecular Dynamics of Protonated Dialanine and Comparison to Infrared Multiphoton Dissociation Experiments. *J. Phys. Chem. A* **2006,** *110,* 8802–8810.
50. Kulhánek, P.; Schalg, E. W.; Koča, J. A Novel Mechanism of Proton Transfer in Protonated Peptides. *J. Am. Chem. Soc*. **2003,** *125,* 13678–13679.
51. Paizs, B.; Csonka, I. P.; Lendvay, G.; Suhai, S. Proton Mobility in Protonated Glycylglycine and N-Formylglycylglycinamide: A Combined Quantum Chemical and RKKM Study. *Rapid Commun. Mass Spectrom*. **2001,** *15,* 637–650.